Yamagata Med J (ISSN 0288-030X) 2022 ; 40(1) : 1 -20
DOI 10.15022/00005304

Five Patterns of Cell Signaling Associated with Cell Behavior

Yuji Takeda*, Kazuharu Kawano*, Rui Ma*,, Shinichi Saitoh*, Hironobu Asao***

*Department of Immunology, Faculty of Medicine, Yamagata University
**Department of Infectious disease medicine, School of Basic Medical Sciences, Ningxia Medical University
(Accepted October 25, 2021)

ABSTRACT

Signal transduction is thought to control flexible cellular responses by combining a specific robust response with a regulatory ability to interact with multiple signals. Previous biophysical studies have proposed that cell behavior be expressed in a multidimensional space with a basin of attractors. Alternatively, flow cytometry analysis provides mean fluorescence intensity (MFI) and coefficient of variation (CV) in an arbitrary cell population. In terms of the biophysical concept, MFI and CV are considered to be the activation energy and cell fluctuations, respectively. In the current study, we present a new approach to understand cell signaling pathways associated with cell behavior linking the above concepts. To link the biophysical concept and flow cytometry data, we measured the phosphorylation levels of signal transducers in a cell and the fluctuation of the phosphorylation level in a population of cells. Topologically, the changes in MFI and CV were categorized into five patterns, which indicated emergent properties of cell behavior. The novel classification method is a simple and effective approach for classifying unknown network systems without using machine learning algorithms or ontology analysis.

Keywords: ocell behavior; cell signaling pathway; emergent property; flow cytometry; phosphorylation

Introduction

Life is a complex phenomenon that combines plasticity and robustness of molecular and other responses. Accordingly, various signaling molecules have been identified and complex signaling mechanisms have been investigated to dissect this complexity[1]. However, in order to understand complex systems, it is necessary not only to apply the molecular reduction method but also to recognize the emergent properties caused by molecular organization.

For a comprehensive understanding of complex systems, comprehensive (-omics) analyses of various hierarchies, such as nucleic acids, proteins, or metabolites, have been performed, and many types of simulation have been constructed to accommodate the amassed data. Recently, transomics, which combines the knowledge of signal transduction mechanisms and databases of -omics analyses with systems biology, has been successfully developed as a tool to understand complex systems[2),3)]. However, these -omics approaches are based on the assumption that a population of cells behaves in a uniform manner.

Although lysis (homogenization) of a cell population is a powerful method for detecting the protein-protein interactions, or an increase or decrease in levels of a small number of molecules, cell population in such experiments is typically treated as a single large cell. However, response heterogeneity is always a factor in experiments that involve biological material; consequently,

mathematical induction proof using statistics is used to decide a significance. The heterogeneous response of a cell population reflects the plasticity of complex systems; however, this response is ignored as an error caused by undetectable early differences or stochastic environmental differences. Therefore, to understand a complex system, heterogeneous responses of a cell population should be analyzed.

To overcome problems associated with sample analysis by lysis, single-cell analysis methods using mass cytometry or next-generation sequencing have been developed[4]. However, these analysis methods also compare based on the amount of increase or decrease of arbitrary parameters, and do not deal with information on the variance of cell populations. When data from single-cell analysis are presented as a higher-dimensional space, the data are reproduced in a two-dimensional space using statistical methods, such as t-distributed stochastic neighbor embedding (*t*-SNE) or uniform manifold approximation and projection (UMAP)[5),6)]. These methods help to identify new cell populations, but their novelty depends on the number of parameters (number of gene types) and the amount of data (number of cells). As the analyzed gene types (or number of cells) increases, new cell populations continue to emerge. Furthermore, these low-dimensional processing by these statistical processing methods does not maintain the dispersion of the cell population for one parameter. In addition, as far as I know, there is no multidimensional analysis using the variance of cell signaling in a cell population. Diffusion maps and Bayesian approaches are often used for cell clustering in single-cell analyses. It is perfectly fine to apply diffusion maps and Bayesian approaches for force and optical correction of physical mechanical events in cells. It is also possible to make up for missing data using physical, mechanical and statistical methods to classify the emergent characteristic behavior of cells as a novel population of cells. However, if we assume that the emergent properties of the cellular response consist of reactions that differ from molecule to molecule, such as enzyme substrate specificity, receptor specificity, and mRNA stability, this assumption contradicts the method of mechanical calculation relying on uniform physical dynamics and statistical algorithms.

Module analysis using ontology is another approach for correcting data variability. However, non-verbalized events (events that are unrecognized or related to many other events, etc.) are excluded from ontology analysis. The ontology analysis is used to explain a discovered phenomenon, instead of detecting a novel phenomenon. Perhaps it is currently not possible to verify the emergent properties of cell behavior to understand complex systems using single-cell analysis.

Kaneko et al. devised various biophysical theories and proposed a model focusing on cell behavior[7)-9)]. They proposed that cell behavior is regulated by "attractors" and "basins" in a higher dimensional space. In the current study, we focused on cell signals as representative phenomena of cell response and attempted to establish a method for classifying cell behavior based on bio-physical theory using flow cytometry (FCM) analysis. We attempted to integrate the bio-physical assumptions with FCM measurements, which have been shown to be a useful tool for verifying the emergent properties of cell behavior. These findings will be a simple and effective approach for classifying unknown network systems.

The biophysical theory is explained as follows. A cell receives many signals from the extracellular milieu and responds to these signals. According to the biophysical theory, the behavior of a cell can be expressed in multi-dimensional space X, as shown by the X1, 2... k axes in Figure 1a. These X-axes are parameters defined by each experimental observation. A cell (small ball) freely moves in space X. It is attracted to a basin (ψ_1 or ψ_2) of attractors, indicating that it responds to some signals. Many attractors in space X perturb cell movement. The cell is trapped for a relatively long time by a strong attraction (dashed arrow of ψ_1, Figure 1a), indicating a robust cell response. However, a weak attraction cannot trap the cell for a long time in the basin (dashed arrow of ψ_2, Figure 1a), indicating that the cell is susceptible to other attractors. Therefore, weak attractors possess a large basin range and strong attractors possess a small basin

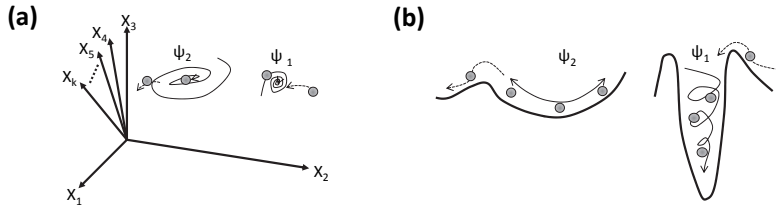

Figure 1. Schematic representation of the theoretical relationship between cell behavior and an attractor. A cell (gray ball) moves freely in space X. When the cell responds to ψ_1 or ψ_2, it is attracted to ψ_1 or ψ_2. The trapping of a cell in ψ_1 or ψ_2 is indicated by whorled arrows. The basin of attraction is reflected in the fluctuation of the moving cell. Cell transiting to another basin is indicated by dashed arrows. The attractive power of ψ_1 is stronger than that of ψ_2. (a) Schematic representation of cell behavior in the multiparametric space X. (b) Schematic representation of cell behavior considering a single parameter. The basins of attraction are presented as valleys and mountains. The attractive powers are presented as the valley depth. These diagrams summarized past studies that Kaneko *et al.* devised various biophysical theories and a model on cell behavior [7)-9)].

range. The basin ranges are fluctuations.

When the basins (ψ_1 or ψ_2) are observed from a suitable axis, they are either seen as valleys or mountains (Figure 1b). The power of attraction is represented by the valley depth. Removal to another valley requires a significant amount of energy, which is considered the height of a mountain. This theoretical cell behavior has been proposed in previous biophysics studies[10]. Furthermore, it is evident that the amount of energy is equivalent to the level of activated signaling pathways, such as ion influx, electron transfer, or protein phosphorylation.

Materials and Methods

Human Peripheral Blood Sampling

All methods were performed in accordance with the relevant guidelines and regulations. All healthy volunteers signed an informed consent form prior to the blood collection. This study was approved by the Ethics Committee of Yamagata University Faculty of Medicine (Yamagata, Japan; approval number: H28-265). Peripheral blood was collected from the brachial vein and heparinized with 5 U/mL of low-molecular-weight heparin. The average age of the volunteers was 47.0 ± 1.6 years (n = 5, male). Following sample collection, the blood was immediately transferred into 1.5-mL microtubes and used for experiments.

Cell Lines

HL-60 cells were obtained from the JCRB Cell Bank of the National Institutes of Bio-medical Innovation, Health and Nutrition (Tokyo, Japan). U937 cells were a gift of Prof. N. Ishii (Department of Immunology, Tohoku University School of Medicine, Sendai, Japan). These cells were maintained in RPMI 1640 medium (Sigma-Aldrich, St. Louis, MO). The culture media were supplemented with 10% (v/v) heat-inactivated fetal calf serum (Biowest, Nuaillé, France), 50 U/mL penicillin G potassium, and 50 μg/mL streptomycin sulfate. The cell lines were cultured at 37℃ and 5% CO2 in a high-humidity chamber.

Antibodies

The following antibodies were used in the current study: Pacific Blue-conjugated anti-human CD3 mAb (UCHT1), phycoerythrin (PE)-conjugated anti-Bcl-6 mAb (7D1), and Alexa647-conjugated anti-phosphorylated tyrosine mAb (PY20), from BioLegend (San Diego, CA); fluorescein isothiocyanate (FITC)- or PE-conjugated anti-human CD14 mAb (MψP9), Alexa488-conjugated anti-pY701-STAT1 mAb (4a), Alexa488-conjugated anti-pY705-STAT3 mAb (4/P-STAT3), Alexa488-conjugated anti-pY694-STAT5 mAb (47/Stat5), Alexa647-conjugated anti-pT202/pY204-ERK1/2 mAb (20A), V450-conjugated anti-pS473-Akt mAb (M89-61), and Alexa488-conjugated anti-pT180/pY182-p38MAPK mAb (36/p38), from BD Biosciences (Franklin Lakes, NJ); PE-conjugated anti-GPI-80

mAb (3H9), from MBL (Nagoya, Japan); Alexa647-conjugated or non-conjugated anti-pS536-NF-κBp65 rabbit mAb (93H1), from Cell Signaling Technology (Beverly, MA); and Alexa488-conjugated goat anti-rabbit IgG Ab, from Thermo Fisher (Molecular probes, Eugene, OR). As mouse control mAbs, IgG1 (MOPC-21) and IgG2a (G155–178) were used, from BD Biosciences and BioLegend, respectively.

Cytokines and Stimulants

IFN-α and G-CSF were purchased from Takeda Pharmaceutical Co. Ltd (Osaka, Japan) and Chugai Pharmaceutical (Tokyo, Japan), respectively. IL-21 was purchased from Peprotech (Rocky Hill, NJ). LPS from Escherichia coli O127:B8 and PMA were purchased from Sigma-Aldrich.

Stimulation of Cell Lines and Whole-blood Cells

Cell stimulation was performed as previously reported[11]. Briefly, HL60 and U937 cells (2×10^5 cells/mL, 1 mL/tube) were preincubated in 1.5 mL microtubes for 60 min at 37℃ in RPMI 1640 containing 10% fetal calf serum. Whole peripheral blood cells were transferred into microtubes (0.3 mL) and preincubated for 20 min at 37℃. After the addition of various stimulants, the microtubes were immediately vortex-mixed for few seconds and incubated at 37℃ in a heat block for the indicated times. After stimulation, the cells (1 mL) were immediately fixed by the addition of 0.2 mL of 5× Lyse/Fix buffer (BD Biosciences) for 10 min at 37℃. Whole-blood cells (0.1 mL) were immediately fixed by suspending in 1.4 mL of 1× Lyse/Fix buffer (BD Biosciences) for 10 min at 37℃. The fixed cells were collected by centrifugation at 800 × g for 1 min at 24℃, and then stored in 90% methanol (0.3 mL) at −20℃ until staining with antibodies.

Cell Staining with Antibodies and FCM Analysis

The fixed cells were washed with 0.8 mL of phosphate-buffered saline (PBS), and suspended in PBS containing 3% fetal calf serum and 0.1% sodium azide. The cells were incubated with each antibody for 45 min at 22–25℃ after Fc receptor blocking using an Fc blocker (Human TruStain FcX, Biolegend). After the reaction, the cells were washed with PBS and analyzed by FCM (ec800, Sony, Tokyo, Japan, or FACSCanto II, BD Biosciences, as indicated). Cell debris was excluded from the analysis by forward- and side-scatter gating. MFI and robust CV were analyzed using FlowJo software (version 7.6.5, TreeStar, Ashland, OR). FlowJo software calculates the robust CV using the following formula: CV = 100 × 1/2 [(intensity at 84.13 percentile) − (intensity at 15.87 percentile)] / Median. The number of cell events did not affect this calculation.

Statistical Analysis

Data are presented as the mean ± standard error (SE). The calculation of standard deviation (SD) was used for the classification of "Type 3". Statistical analysis was performed using Prism software (version 5.03, GraphPad Software, San Diego, CA). Statistical significance was set at $p < 0.05$.

Results

FCM Observations Reflect Theoretical Cell Behavior

FCM is useful for measuring antigen expression on cells. When cells are stained with a fluorescence-conjugated antibody raised against a phosphorylated molecule from a signaling pathway, FCM analysis can be used to define the activation level of the signaling pathway per cell. Furthermore, the cell data can be used to construct a histogram of activation levels in a cell population. Hence, the coefficient of variation (CV) of the histogram indicates a fluctuation of each data point, corresponding to a basin of an attractor. Furthermore, the mean fluorescence intensity (MFI) is the same as the mean value of the histogram, corresponding to the level of activated signaling pathway in a cell cluster.

In this study, we consider that the variability at the initial observation point and the variability at any observation point are necessary fluctuations as a response of the cell cluster. Therefore, since we can only recognize the amount of change compared between the two points to be observed, we can only recognize the direction of cell behavior between the two points. If the changes between these two points are classified by MFI and CV, they can be classified

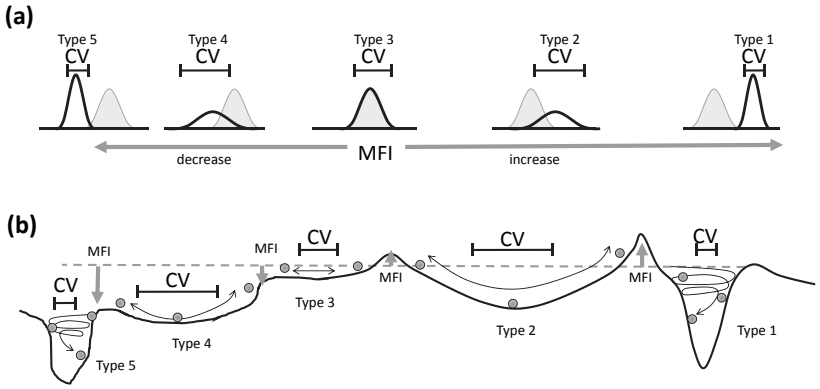

Figure 2. Schematic representation of the theoretical relationship between cell behavior and flow cytometry (FCM) analysis. (a) Five topological histogram patterns from FCM analysis. The gray-filled histograms and open histograms indicate the initial cell status and cell status after receiving a signal, respectively. The latter histogram patterns are topologically categorized into five types (types 1–5) based on the increase or decrease in mean fluorescence intensity (MFI; gray arrows) combined with an increase or decrease in coefficient of variation (CV; range of bars). (b) Relationship between FCM-analyzed parameters (MFI and CV) and theoretical cell behavior. A fluctuation in cells (basin) corresponds to a range of CV, and an amount of energy (height of mountain) is equivalent to the value of MFI. The changes in MFI and CV represent five types of the cells transition.

Table 1. Hypothetical categorization of cells transition by FCM analysis.

Categories	Change in MFI/CV	Provisional name of cells transition
Type 1	MFI↑/ CV↓	Attractive
Type 2	MFI↑/ CV↑	Subsequent
Type 3	unchanged	Passive
Type 4	MFI↓/ CV↑	Counter
Type 5	MFI↓/ CV↓	Negative arbiter

The categories correspond to Fig 2. "↑" or "↓" are indicated as increase or decrease, respectively.

as follows. It is generally assumed that the final state histograms adapt five topologically distinct patterns when compared to the initial state histograms (Figure 2a). In Figure 2a, gray-filled histograms represent the initial state of a signaling pathway. During response to a signal, the histograms change and follow five different patterns: type 1, an increase in MFI and decrease in CV; type 2, an increase in both MFI and CV; type 3, both MFI and CV remain unchanged; type 4, a decrease in MFI and increase in CV; and type 5, a decrease in both MFI and CV.

We considered the relative change in the five histogram patterns to reflect the five types of cells transition (Figure 2b). An MFI increase compared to the initial level (dashed gray line in Figure 2b) indicates that the cell receives a significant amount of energy to move into another basin. An MFI decrease denotes the disappearance of a mountain, meaning that the decrease in energy is fused (disappear of basin) with another basin. The power of attraction is shown as valley depth, which is detected as CV. Therefore, type 1 is responsive to a robust attractor; type 2 is a response to a weak attractor; type 3 is an initial attractor; type 4 is a response to weak attractors counteracting the initial attractor; and type 5 is a level drop to the ground state. We provisionally defined the power of attraction as follows: type 1, "attractive"; type 2, "subsequent"; type 3, "passive"; type 4, "countering"; and type 5, "negative arbiter" (Table 1). This classification has also been proposed in previous reports[12), 13)].

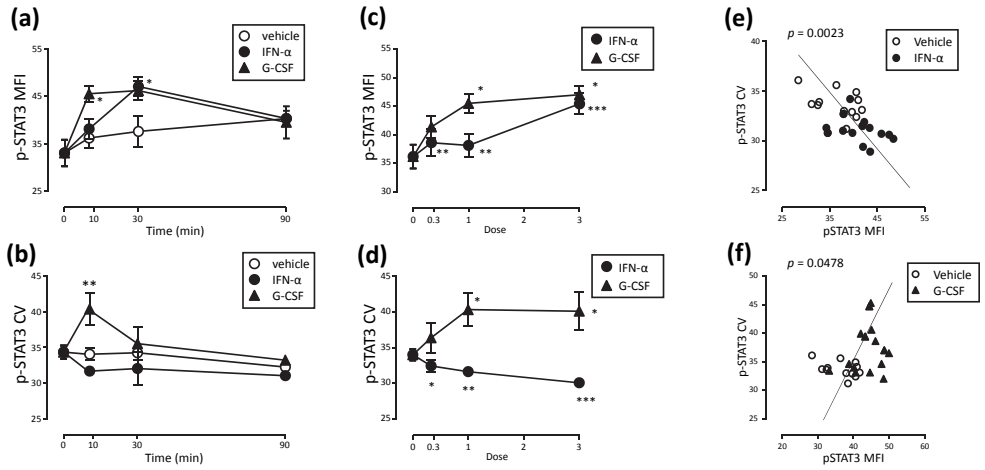

Figure 3. Changes in MFI and CV after cell stimulation with IFN-α or G-CSF. HL60 cells were stimulated with a vehicle (open circle), IFN-α (closed circle), or G-CSF (closed triangle). The cells were stimulated with IFN-α (100 U/mL) or G-CSF (1 nM) for 0, 10, 30, and 90 min (a and b). In another set of experiments, the cells were stimulated with various doses of IFN-α (0.3, 33 U/mL; 1, 100 U/mL; 3, 300 U/mL) or G-CSF (0.3, 0.33 nM; 1, 1, 3, and 3 nM) for 10 min (c and d). After stimulation, the cells were fixed, permeabilized, and stained with Alexa488-conjugated mAb raised against phosphorylated (p) STAT3. The cells were analyzed by FCM (ec800), and MFI (a and c) and CV (b and d) of the resultant histograms determined. Data are represented as the mean ± standard error (SE) from three independent experiments. Statistical analysis was performed using two-way ANOVA with post-hoc test using Bonferroni's correction for comparison to the vehicle in (a) and (b), or one-way ANOVA with post-hoc test using Bonferroni's correction for comparison to the dose of 0 in (c) and (d). $^{*}p < 0.05$; $^{**}p < 0.01$; $^{***}p < 0.001$. (e and f) Correlations between MFI and CV during cell stimulation with IFN-α or G-CSF. HL60 cells were stimulated with a vehicle (open circle; e and f), IFN-α (closed circle; e), or G-CSF (closed triangle; f). The cells were analyzed by FCM (ec800), and p-STAT3 MFI (horizontal axis) and p-STAT3 CV (vertical axis) were determined. The data represent three independent experiments. The statistical significances of correlation were calculated using Pearson's correlation coefficient (*p*-value is indicated in each figure).

Changes in CV Indicate that Differences in Cell Behavior are Stimulant-dependent

Previously, we measured MFI and CV of several phosphorylated signal transducers using FCM[11),13)]. We showed that stimulants or inhibitors induce fluctuations in the phosphorylated signal (change in CV), which is related to the level of phosphorylation (change in MFI)[13)]. However, it is still unclear whether CV is dependent on the character (affinity or specificity) of the antibody used the experiments and whether it is regulated by the stimulant dose.

To test the effect of the antibody and the stimulant dose on CV, HL60 cells were stimulated with interferon (IFN) α or granulocyte colony-stimulating factor (G-CSF). MFI and CV of phosphorylated signal transducer and activator of transcription 3 (p-STAT3) in cells were measured by one type of specific antibody [anti-phosphorylated STAT3 monoclonal antibody (mAb)]. Representative FCM data for HL60 cells are shown in Fig. S1a–c. IFN-α led to increased p-STAT3 MFI, with a peak at 30 min (Figure 3a). Similarly, G-CSF led to increased p-STAT3 MFI, with a peak at 10–30 min (Figure 3a). The same anti-p-STAT3 mAb was used in these experiments. However, G-CSF led to a significantly increased p-STAT3 CV, with a peak at 10 min, while IFN-α did not lead to an increase in p-STAT3 CV during the incubation period (Figure 3b). These observations indicate that the changing CV pattern during cell activation is dependent on the stimulant, but not on the char-acter of the antibody used.

Next, we investigated whether different cytokine concentrations caused different changes in MFI and CV. Cells were stimulated with several doses of IFN-α (33, 100, or 300 U/mL) or G-CSF (0.33, 1, or 3 nM) for 10 min. Stimulation with both IFN-

α and G-CSF significantly increased p-STAT3 MFI in a dose-dependent manner (Figure 3c). However, IFN-α and G-CSF induced opposite changes in the p-STAT3 CV, with IFN-α decreasing p-STAT3 CV and G-CSF increasing p-STAT3 CV (Figure 3d). These observations indicated that the direction of CV change was dependent on the type of stimulus, but not on the stimulant dose, even in the same cell line.

Signaling Pathways that Involve Transient Activation Can Be Distinguished Based on Correlations Between MFI and CV

The activation of a signaling pathway is generally transient. Although statistically significant changes in both MFI and CV are easily detected at the peak of activation, it is unclear whether significant changes in both MFI and CV can also be detected before or after the peak of activation. Logically, when a cell population profile changes from the initial state to type 1 histogram, the increase in MFI is accompanied by a decrease in CV; and when a cell population profile changes from the initial state to type 2 histogram, the increase in MFI is accompanied by an increase in CV. Consequently, a negative correlation between MFI and CV is detected for type 1 (attractive) and a positive correlation between MFI and CV is detected in type 2 (subsequent). Therefore, it is possible that transient and simple activation may be detected based on the correlation between MFI and CV, independent of the observation time.

To test these possibilities, the correlation between MFI and CV was analyzed. We observed that p-STAT3 MFI in cells stimulated with IFN-α or G-CSF transiently increased (Figure 3a). IFN-α exposure slightly decreased CV, with a negative correlation between p-STAT3 MFI and CV (Figure 3e). G-CSF exposure led to a transient increase in CV, with a positive correlation between p-STAT3 MFI and CV (Figure 3f). These analyses provide evidence that a signaling pathway involving transient and simple activation can be distinguished based on the correlation between MFI and CV. Hence, at any time point or during the sum of time points, type 1 (attractive) exhibits a negative correlation between MFI and CV, while type 2 (subsequent) exhibits a positive correlation between these parameters.

Because types 4 and 5 are mirror images of types 2 and 1, respectively, the positive or negative correlations can also be applied to transient deactivation (i.e., temporal decrease in MFI) to type 4 (countering) or type 5 (negative arbiter), respectively.

Signaling Pathways with Oscillating Activation Can Be Recognized by Persistence of Type 2 (Subsequent) Without a Positive Correlation Between MFI and CV

Activation of nuclear factor (NF)-κB is controlled in an oscillatory manner to regulate its biological function[14]. We asked if this oscillating-activation signaling pathway can be recognized using FCM. It is known that the level of NF-κB activation in the early phase (t_1) is higher than that in the late phase (t_2) of response (Figure 4a). Thus, the oscillation pattern indicates that cell movement from the initial basin (ψ_0) to another basin (ψ_1) will occur in the early phase (t_1) but not in the late phase (t_2), as shown in the conceptual schema in Figure 4b. If the oscillation is highly synchronized in a cell population, the oscillation signal should be simply detected as oscillatory changes in MFI with-out changes in CV. However, oscillatory changes are not generally synchronized in a cell population. Therefore, the amplitudes should be accompanied by an increase in CV (Figure 4b), indicating that the persistence of oscillation should be recognized as an increase in CV compared to the initial CV status (t_0 vs. t_1 or t_2; Figure 4b). Furthermore, the amplitudes in the late phase are smaller than the amplitudes in the early phase (Figure 4a), indicating that MFI in the late phase should be lower than that in the early phase (t_1 vs. t_2; Figure 4b). In summary, the oscillation signal is detected as the persistence of an increase in both MFI and CV (type 2), with a decrease in MFI in the late phase.

To verify this hypothesis, the levels of phosphorylated p65 NF-κB (p-p65 NF-κB) MFI and p-p65 NF-κB CV were determined in U937 cells stimulated by phorbol myristate acetate (PMA). Representative FCM data for U937 cells are shown in Figure S1d–f. The in-crease in p-p65 NF-κB MFI

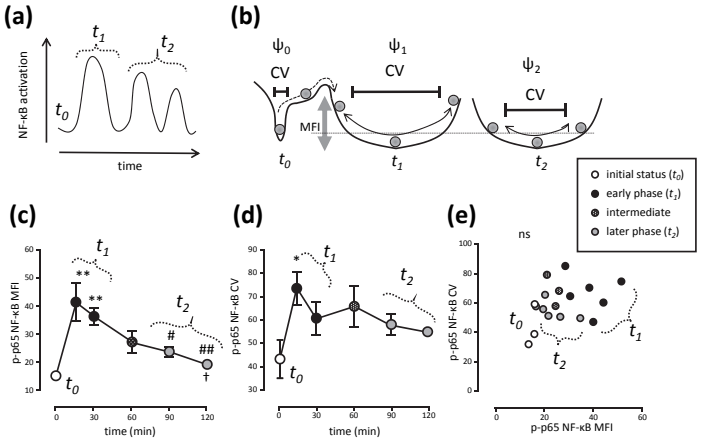

Figure 4. Analysis of the oscillatory signal of nuclear factor (NF)-κB using flow cytometry (FCM). (a) Schematic representation of oscillatory NF-κB activation according to a previous report [14]. After stimulation, NF-κB is quickly activated from the initial status (t_0) in the early phase (t_1). The activation gradually decreases in the late phase (t_2). (b) Schematic representation of the relationship between oscillatory cell behavior and FCM analysis (MFI and CV). The transition of a phosphorylated (signaling) cell into an oscillatory basin (ψ_1, t_1) from the initial basin (ψ_0, t_0) in the early phase is indicated by dashed arrows. The amplitudes in the oscillatory basin (ψ_1) decrease depending on the level of phosphorylation in the late phase (t_2). (c and d) Changes in phosphorylated p65 NF-κB (p-p65 NF-κB) levels in activated U937 cells. The cells (2×10^5 cells/mL) were stimulated with PMA (100 ng/mL) for 15, 30, 60, 90, and 120 min. After stimulation, the cells were fixed, permeabilized, and stained with rabbit anti-p-p65 NF-κB mAb and Alexa488-conjugated goat anti-rabbit polyclonal Ab. The cells were analyzed by FCM (ec800), and changes in p-p65 NF-κB MFI (c) and p-p65 NF-κB CV (d) were determined. Statistical significance was calculated by one-way ANOVA with post-hoc by Tukey's test (n = 3), $^{*}p < 0.05$, $^{**}p < 0.01$, compared to 0 min; $^{\#}p < 0.05$, $^{\#\#}p < 0.01$, compared to 15 min; †$p < 0.05$, compared to 30 min. There was no significant difference among the other pairs (not indicated). (e) Correlations between p-p65 NF-κB MFI and p-p65 NF-κB CV. The statistical significance of correlations was calculated with Pearson's correlation coefficient (not significant, ns).

stimulated by PMA was accompanied by an increase in p-p65 NF-κB CV in the early phase (t_0 compared to t_1; Figure 4c, d). After the early phase, the levels of p-p65 NF-κB MFI decreased significantly depending on the time point in the late phase (t_1 compared to t_2; Figure 4c). Similarly, p-p65 NF-κB CV decreased in the late phase, but not significantly (t_1 compared to t_2; Figure 4d). These changes in MFI and CV were categorized as follows: the change between t_0 and t_1 was an increase in both MFI and CV, indicating a typical type 2 pattern (subsequent); the change between t_1 and t_2 was a decrease in MFI; and the change between t_0 and t_2 was an increase in both MFI and CV, which was type 2 pattern (subsequent). Overall, the oscillation signal was recognized as an increase in both MFI and CV, representing type 2 (subsequent). During the entire observation period from t_0 to t_2, no correlation between MFI and CV was apparent (Figure 4e) because type 2 and type 4/5 (an intermediate between countering and a negative arbiter) were mixed in the time point. These observations indicate that the categorization using FCM can be used to class the oscillating signaling pathway as "type 2 and no correlation".

Homeostatic extracellular signal-regulated kinase 1/2 (ERK1/2) Pathway is a Special Type 3 (Passive) Pattern with a Constant Negative Correlation Between MFI and CV

Type 3 (passive) belongs to a category in which the stimulatory and initial states are not significantly different (Figure 2, Table 1). Previously, we reported a negative correlation between phosphorylated ERK1/2 (p-ERK1/2) MFI and p-ERK1/2 CV in Jurkat cells, without significant changes in either MFI or CV[13].

In the current study, we measured p-ERK1/2 levels in human neutrophils and T cells in whole

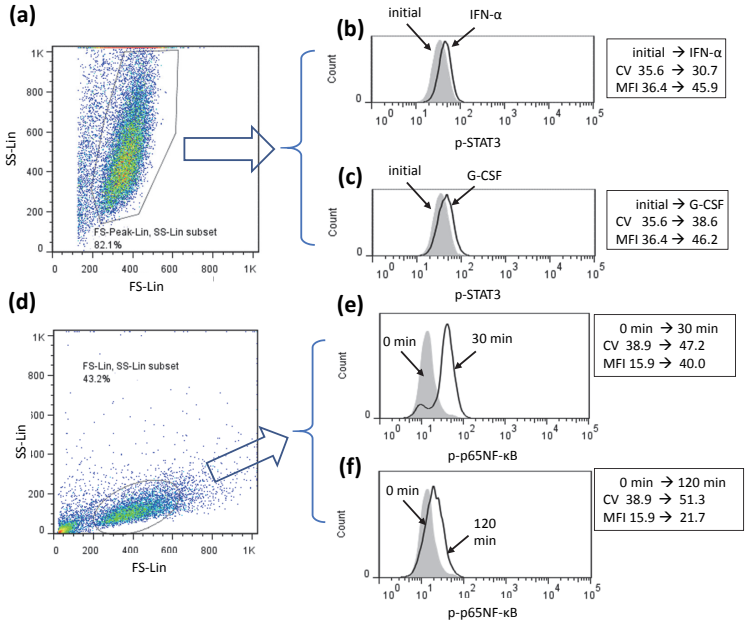

Figure S1. Representative gating strategy for HL60 cells and U937 cells. HL60 cells (a–c) were analyzed by flow cytometry (ec800). (a) Gating for the exclusion of cell debris and aggregated cells (FS-Lin vs. SS-Lin). The gated cell population is presented on the histograms for phosphorylated signal transducer and activator of transcription 3 (p-STAT3) data, as p-STAT3 (horizontal axis) in (b) and (c). The gray-filled histograms represent the initial state of the cells (0 min), and the open black histograms in (b) and (c) indicate cells stimulated for 10 min with 300 U/mL interferon (IFN)-α or 3 nM granulocyte colony-stimulating factor (G-CSF), respectively. U937 cells (d–f) were also analyzed by flow cytometry (ec800). (d) Gating for the exclusion of cell debris and aggregated cells (FS-Lin vs. SS-Lin). The gated cell population is presented on the histograms for phosphorylated p65NF-κB (p-p65NF-κB) data, as p-p65NF-κB (horizontal axis) in (e) and (f). The gray-filled histograms represent the initial state of the cells (0 min), and the open black histograms in (e) and (f) indicate cells stimulated with 100 ng/mL phorbol myristate acetate (PMA) for 30 min or 120 min, respectively. The raw data (mean fluorescence intensity, MFI; and robust coefficient of variation, CV) are presented in the rectangle on the right side of each histogram.

peripheral blood stimulated with various cytokines, such as IFN-α, interleukin (IL) 21, and G-CSF, alone or in combination, to confirm the negative correlation. Although IFN-α and IL-21 primarily activate STAT3 pathways, these cytokines simultaneously activate the ERK pathway in various cell types[15),16)]. G-CSF also primarily activates STAT3 and concomitantly activates the ERK pathway in myeloid cells[17)]. Whole blood was stimulated with these cytokines, and p-ERK1/2 levels were analyzed in GPI-80+ cells (neutrophils). Representative FCM data for T cells and neutrophils in the peripheral blood are shown in Figure S2. The various stimulations and cytokine combinations tested did not significantly change either MFI or CV of p-ERK1/2 in neutrophils (Figure 5a, b) and T cells (Figure S3a, b). These observations indicate that the ERK1/2 pathway in both T cells and neutrophils is a type 3 (passive) pathway under all conditions tested. Interestingly, these analyses revealed a significantly negative correlation between p-ERK1/2 MFI and p-ERK1/2 CV (Figure 5c and Figure S3c). The negative correlation without a significant increase in MFI indicated the existence of persistently controlled signals without an increase in the moving energy. The ERK pathway, which plays a crucial role in cell survival, induces asynchronous pulses of varying frequencies and durations[18),19)]. Hence, the negative correlation without an MFI increase may indicate cell survival signals, i.e., "homeostatic" ERK pathway.

To verify that type 3 (passive) pathway with a negative correlation is the homeostatic ERK pathway, we compared the emergent response via the ERK pathway, i.e., an inflammatory response

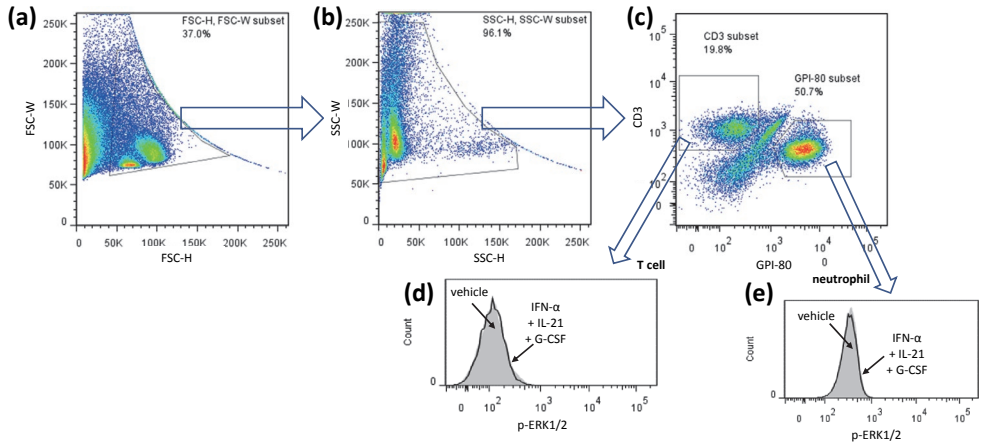

Figure S2. Representative gating strategy for human T cells and neutrophils. Whole-blood cell samples were analyzed by flow cytometry (FACSCanto II). (a) Gating for the exclusion of erythrocytes and cell ghosts (FSC-H vs. FSC-W). (b) After the step described in (a), the gated cells were re-gated according to SSC-H vs. SSC-W. Gating for the exclusion of cell debris and aggregated cells is also shown here. (c) Gating for the selection of $CD3^+$ T cells or GPI-80+ neutrophils (CD3 vs. GPI-80). The T-cell or neutrophil populations are presented on the histograms for phosphorylated extracellular signal-regulated kinase 1/2 (p-ERK1/2) data, as p-ERK1/2 (horizontal axis) in (d) and (e), respectively. The gray-filled histograms are the initial state (vehicle) of p-ERK1/2, and the open black histograms indicate cells stimulated with 100 U/mL IFN-α + 1 nM interleukin (IL)-21 + 1 nM G-CSF for 30 min. The open black histograms almost overlap with the gray-filled histograms in both (d) and (e).

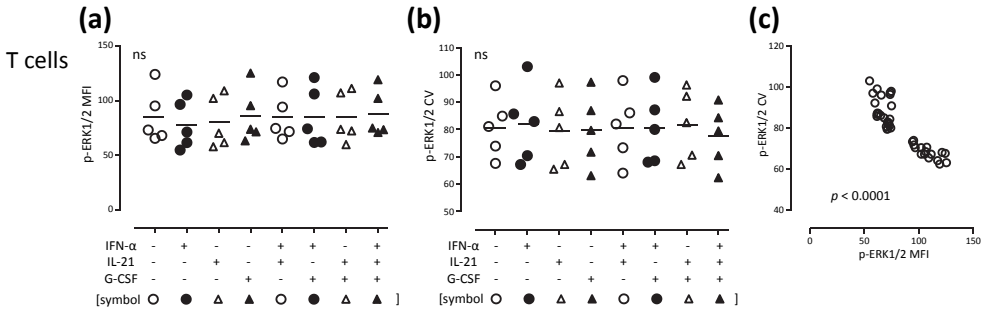

Figure S3. Analysis of the homeostatic ERK pathway in T cells. Human peripheral blood cells were stimulated with IFN-α (100 U/mL), IL-21 (1 nM), or G-CSF (1 nM), or a combination of these cytokines for 30 min. After stimulation, the cells were fixed, permeabilized, and stained with Pacific Blue-conjugated anti-human CD3 mAb and Alexa647-conjugated anti-phosphorylated ERK1/2 mAb. The cells were analyzed by flow cytometry (FACSCanto II). $CD3^+$ cells were gated for T-cell analysis (a–c). MFI (a) and CV (b) of phosphorylated ERK1/2 (p-ERK1/2) were analyzed. Data were obtained from four independent experiments, and statistical significance was calculated using one-way ANOVA (not significant, ns). (c) Correlation between MFI and CV. The statistical significance of the correlation was calculated using the Pearson's correlation coefficient ($p < 0.0001$).

induced by lipopolysaccharide (LPS)[20),21)]. Whole blood was stimulated with LPS, and p-ERK1/2 levels were analyzed in $CD14^+$ monocytes. Representative FCM data for monocytes in the peripheral blood are shown in Figure S4. Both p-ERK1/2 MFI and p-ERK1/2 CV increased significantly after LPS stimulation, that is, indicating type 2 (subsequent) (Figure 5d). Furthermore, the correlation be-tween p-ERK1/2 MFI and p-ERK1/2 CV was not detected (Figure 5e), suggesting that the "subsequent and no correlation" pattern showed oscillatory activation similar to the NF-κB pathway in U937 cells stimulated with PMA (Figure 4e). The ERK pathway is an oscillating signaling pathway[22)].

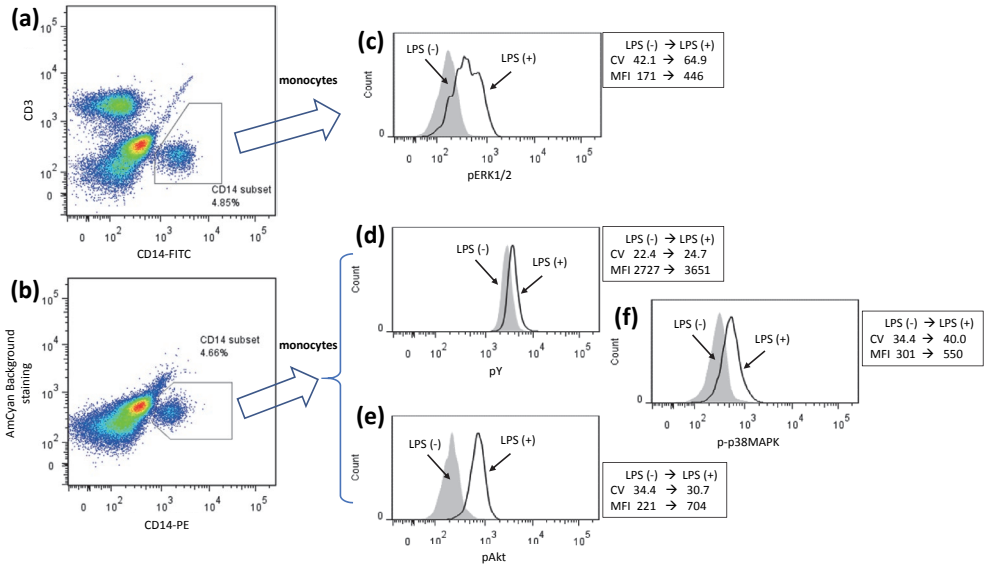

Figure S4. Representative gating strategy for human monocytes. Whole-blood cell samples were analyzed by flow cytometry (FACSCanto II). To exclude erythrocytes, cell ghosts, cell debris, and aggregated cells, gating was performed as shown in Figure S2. The CD14 vs. CD3 (a) and CD14 vs. AmCyan background staining (b) panels show gating for the selection of monocytes. The monocyte population is presented on the histograms for phosphorylated ERK1/2 (p-ERK1/2) (c), phosphorylated tyrosine (p-Y) (d), phosphorylated Akt (p-Akt) (e), or phosphorylated p38MAPK (p-p38MAPK) (f). The gray-filled histograms represent cells treated with a vehicle [lipopolysaccharide (LPS) (–)] for 30 min, and the open black histograms indicate cells stimulated with LPS [LPS(+)] for 30 min. The raw data for each histogram (MFI and CV) are presented in a rectangle on the right side of each histogram.

These observations indicate that the behavior of the ERK pathway shows two different signaling types, oscillating type 2 and homeostatic type 3, depending on the stimulant and cell type.

Detection of Regulatory and Robust Signaling Pathways

The network of signaling pathways consists of many signaling modules. These signaling modules act either coordinately or independently. The interaction of these modules is considered to induce various plasticity responses[1]. We asked whether the FCM-based categorization could be useful for detecting coordinate modules (regulatory signaling pathways) or independent modules (robustness signaling pathways).

Theoretically, robustness is a small basin and perturbed fluctuation is a large basin (Figure 1), indicating that robust or regulatory pathways fall into types 1 or 2, respectively. Previously, it was demonstrated that the phosphatidylinositol 3-kinase-Akt pathway limits LPS activation of signaling pathways (i.e., MAPK/ERK pathway) in human monocytes[23]. Therefore, we speculated that the Akt pathway is a robust signaling pathway, and that the MAPK/ERK pathway, which is regulated by the Akt pathway, is a perturbed regulatory signaling pathway.

To verify the correspondence between changes in CV and the above types of signaling pathways, phosphorylation of Akt and p38 MAPK in monocytes was analyzed using FCM (Figure 6). Following LPS stimulation, changes in phosphorylated p38 MAPK (p-p38MAPK) indicated type 2 (subsequent) pattern, which is a category with an increase in both MFI and CV, similar to that observed for p-ERK1/2 (Figure 5c and Figure 6a). Phosphorylated Akt (p-Akt) was categorized as type 1 (attractive), which is a category with an increase in MFI and a decrease in CV (Figure 6b). These observations suggest that the initial hypothesis was consistent with previous observations of LPS signaling modules.

Further, we analyzed total phosphorylated tyrosine (p-tyrosine) levels in monocytes. Conceptually, an increase in module interaction can be detected as the

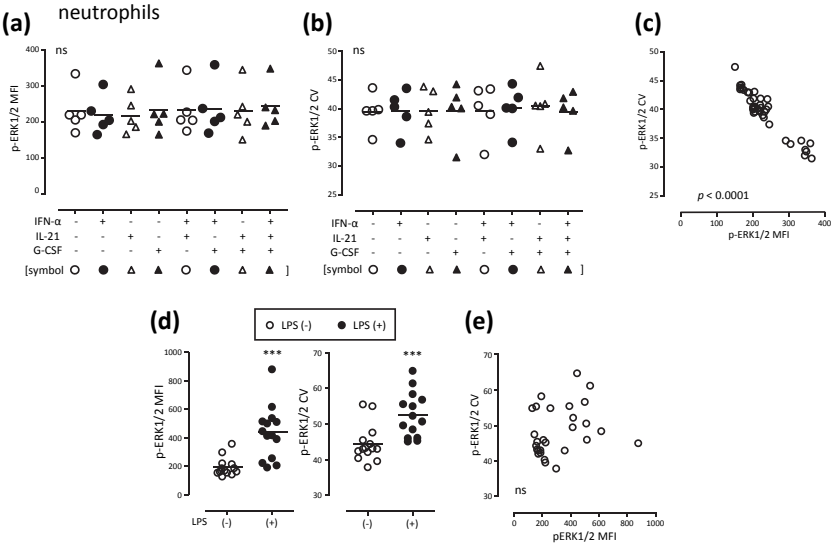

Figure 5. Analysis of the homeostatic and emergent ERK pathway using FCM in human peripheral blood. (a–c) Human peripheral blood cells were stimulated with IFN-α (100 U/mL), IL-21 (1 nM), G-CSF (1 nM), or a combination of these cytokines for 30 min. After stimulation, the cells were fixed, permeabilized, and stained with PE-conjugated anti-GPI-80 mAb, and Alexa647-conjugated anti-phosphorylated ERK1/2 mAb. The cells were analyzed by FCM (FACSCanto II). GPI-80+ cells were gated as neutrophils, and phosphorylated ERK1/2 (p-ERK1/2) signals were analyzed. The MFI and CV values of neutrophils are shown in (a) and (b), respectively. Data were obtained from four independent experiments, and the statistical significance was calculated by one-way ANOVA (not significant, ns). (c) Correlation between MFI and CV. The statistical significance of the correlation was calculated with Pearson's correlation coefficient ($p < 0.0001$). (d,e) Human peripheral blood cells were stimulated (+) or not (−) with LPS (1μg/mL) for 30 min. After the stimulation, the cells were fixed, permeabilized, and stained with FITC-conjugated anti-human CD14 mAb and Alexa647-conjugated anti-phosphorylated ERK1/2 (p-ERK1/2) mAb. (d) MFI and CV of phosphorylated ERK1/2 (p-ERK1/2) in gated CD14+ monocytes, determined by FCM (FACSCanto II). Data were obtained from four independent experiments, and the statistical significance was calculated by Wilcoxon signed-ranks test, $^{***}p < 0.001$ compared to LPS (−). (e) Correlation between MFI and CV. Data were obtained from four independent experiments, and the statistical significance was calculated by Pearson's correlation coefficient (not significant, ns).

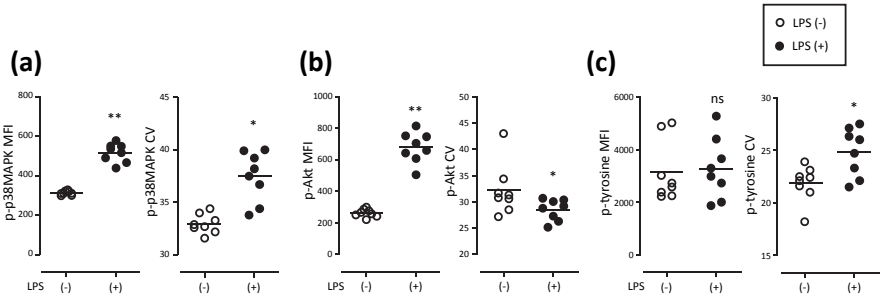

Figure 6. Analysis of regulatory and robust signaling pathways in monocytes using FCM. Human peripheral blood cells were stimulated (+) or not (−) with LPS (1μg/mL) for 30 min. After stimulation, the cells were fixed, permeabilized, and stained with PE-conjugated anti-CD14 mAb, Alexa488-conjugated anti-phosphorylated p38 MAPK (p-p38MAPK) mAb, V450-conjugates anti-phosphorylated Akt (p-Akt) mAb, and Alexa647-conjugated anti-phosphorylated tyrosine (p-Y) mAb. MFI and CV of p-p38MAPK (a), p-Akt (b), or p-Y (c) in gated $CD14^+$ monocytes were determined using FCM (FACSCanto II). Data were obtained from four independent experiments, and statistical significance was calculated using the Wilcoxon signed-rank test, $^{*}p < 0.05$; $^{**}p < 0.01$; $^{***}p < 0.001$ compared to LPS (−).

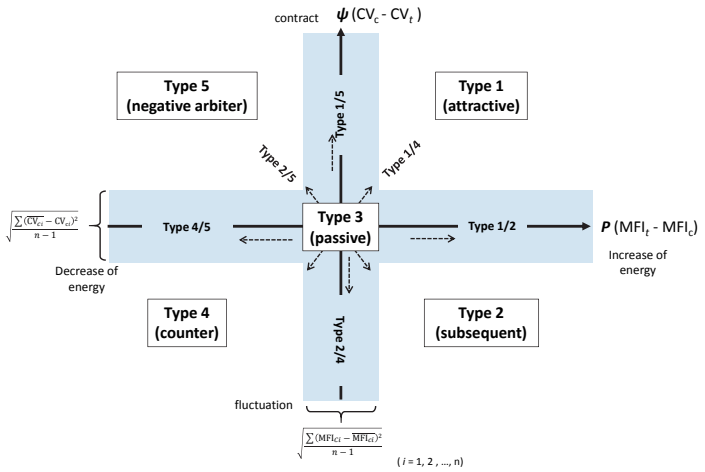

Figure 7. Representation of cell behavior on a P – ψ graph. The increase and decrease in energy, and contraction and fluctuation of deviation are shown. The horizontal axis is P (P = MFIt – MFIc), and the vertical axis is ψ (ψ = CVc – CVt). The five main categories are indicated for each referring to a pattern type. "Type 3, Passive" range is shown as standard deviation (SD) of MFIc and SD of CVc (light blue area). The six separations of type 3 are indicated by dashed arrows.

appearance of several basins around the initial basin or a decrease in the height of the mountain (fusion of basins). Many signal modules involve p-tyrosine, and the interaction between these modules would increase during the emergent response, such as stimulation with LPS. Therefore, we examined whether p-tyrosine CV increased upon interaction of LPS-induced signal modules in monocytes. The total p-tyrosine levels (p-tyrosine MFI) were not significantly altered when monocytes in peripheral blood were stimulated with LPS (Figure 6c). This outcome was reasonable because p-tyrosine MFI represents the sum of many types of signal modules containing phosphorylated and dephosphorylated tyrosine. However, p-tyrosine CV increased significantly (Figure 6c). These observations demonstrate that the increase in CV is adaptable to the increase in signal module interaction.

Simple Mathematical Modeling of Cell Behavior Using CV and MFI

Currently, protein expression, transcription factor activation, mRNA expression, molecular conjugation, enzyme activation, oxidation, intracellular calcium, pH, active oxygen production, cell division, and phagocytosis can be measured as a fluorescence change. Further, not only the behavior of intracellular molecules but also highly hierarchical cell functions, such as the ability to generate reactive oxygen species, cell division, phagocytic ability, and respiratory metabolism can be measured as fluorescence fluctuations. By measuring the fluorescence change using FCM, the MFI and CV values can be easily determined for various phenomena. Therefore, we attempted to apply the above MFI and CV classification to various phenomena by mathematical modeling, as follows.

When an event is observed, it is denoted as a parameter change (P). In the case of FCM analysis, P can be represented by the MFI change. Therefore, P can be determined by subtracting the control (initial) value (c) from the tested value (t). That is,

$$P = \mathrm{MFI}_t - \mathrm{MFI}_c.$$

In the current study, based on the concepts of biophysics (Figure 1), we assumed that the cell behavior deviates from the initial attractor and is captured by another attractor. When an event occurs, the size of the basin changes (ψ). Therefore, ψ can be determined by subtracting the tested value (t) from the control (initial) value (c). That is,

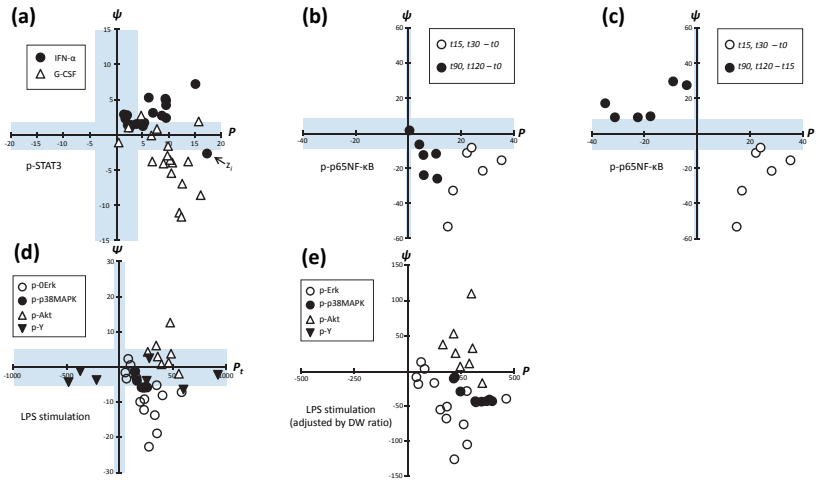

Figure 8. Simple mathematical modeling of cell behavior using CV and MFI and the $P - \psi$ graph. (a) $P - \psi$ graph constructed using data for HL60 cells shown in Figure 3. (b, c) $P - \psi$ graph constructed using the data for U937 cells shown in Figure 4. (b) Observation from the time point t_0 (the difference compared to t_0). (c) Observation from the time point t_0 or t_{15} (the difference between t_0 and t_{15}). (d) $P - \psi$ graph constructed using data for peripheral blood monocytes shown in Figures 5 and 6. The values of P and ψ in (d) were adjusted by "(d, W) ratio", and are presented in (e).

$$\psi = \mathrm{CV}_c - \mathrm{CV}_t.$$

Herein, the elements of cell behavior were classified as shown in Table 1. The classification can be visually presented as a $P - \psi$ graph, with P on the horizontal axis and ψ on the vertical axis (Figure 7).

When an event cannot stochastically deviate from fluctuations in the control (initial) values (MFI_c and CV_c), it is classified as type 3 (passive). For convenience, the standard deviation (SD) of the average value of each repeated measurement (i = 1, 2,⋯, n) of MFI_c or CV_c, subtracted from each control value (c_i) is represented on the $P - \psi$ graph. That is,

$$\text{SD of } P = \sqrt{\frac{\sum(\overline{\mathrm{CV}_c i} - \mathrm{CV}ci)2}{n-1}} \text{ and SD of } \psi = \sqrt{\frac{\sum(\mathrm{MFI}_{Ci} - \overline{\mathrm{MFI}_{ci}})2}{n-1}}.$$

The results of IFN-α and G-CSF stimulation of HL60 cells (Figure 3) can be presented as the $P - \psi$ graph shown in Figure 8a. STAT3 phosphorylation by IFN-α stimulation is type 1 (attractive) class, and STAT3 phosphorylation upon G-CSF stimulation is type 2 (subsequent). In addition, there is an outlier (z_i) in the repeated measurements. It may have been perturbed by a different, unexpected, attractor. The outlier is usually ignored because it is considered an experimental error. However, if z_i changes the $P - \psi$ graph classification, this indicates the existence of a different attractor related to the regulatory perturbation from the perspective of the biophysical theory.

The problem of occurrence (existence) of biological events is described below. The occurrence is problematic because of the infinite number of observation points. Infinite observation points exist not only for elapsed-time observation, but also at various infinite observation points, such as the concentration gradient and the expression level of various molecules. Because the experimental measurement system compares the observation points arbitrarily set from the infinite observation points with other arbitrary observation points, the event is recognized infinitely, depending on the observation point. Infinite existence is a limitation of philosophical recognition. As long as only the increase or decrease of P is measured, and the analysis becomes increasingly high-dimensional, the infinite existence continuously increases and cannot be proven.

Alternatively, the $P - \psi$ graph classification can indicate the occurrence of an event. When the fluctuation of a cell population converges (ψ is increased, and $\psi > 0$), it indicates an attraction. For example, NF-κB activation was classified as a type 2 (subsequent) pattern at 15–30 min and 90–120 min, compared to 0 min. The observation point cannot be ruled out as an infinite event because the type 2 pattern corresponds to a continuous increase in P and a continuous decrease in ψ. However, when 15 min was used as a control point, 90 to 120 min time points were classified as negative arbiters, which is a robust phenomenon (Figure 8b, c). In other words, P and ψ changed discontinuously, and ψ increased after 15 min. An event exists when we can find an observation perspective where $\psi > 0$.

When comparing multiple events ($P_{1,2,\cdots,k}$) by showing them on the same graph, it is difficult to compare the MFI and CV values. For instance, the measurement sensitivity is different for each antibody. Therefore, it is necessary to correct MFI and CV for each k type of measurement conditions. How can k multiple events (P_k) be compared simultaneously? In the current study, we propose the following correction method: If it is assumed that the same stimuli (energy) are given to Pk, and if MFI_t and CV_t are significantly different from MFI_c and CV_c, in other words, if they are not classified as type 3 (passive), the following formula can be used to adjust the values of MFI and CV. The distance (D) difference between the average MFI_c and the average MFI_c is adjusted by the absolute value of P per average MFI_c. That is,

$$D = |\overline{MFI_t} - \overline{MFI_C}| / \overline{MFI_C}.$$

Similarly, the wide (W) histogram difference between the average CV_t and average CV_t is corrected by the absolute value of ψ per average CV_c. That is,

$$W = |\overline{CV_t} - \overline{CV_C}| / \overline{CV_C}.$$

This is based on the premise that the given energies are the same. Thus, the correction is made on the premise that the ratio of the fluctuation difference of the experimental group to the control group occurs to the same extent. An example of such an observational situation is the experiment in which we evaluated multiple signal transduction systems during LPS stimulation, as shown in Figures 5d and 6.

The drawback of this correction method is that if there is not statistically significantly different from the control group (in the case of type 3, passive, pattern), the correction will be excessive and, therefore, cannot be applied. In the current study, the D value was in the range of 0.1 to 1.5, and the W value was in the range of 0.01 to 0.2. MFI and CV of p-ERK1/2, p-p38MAPK, and p-Akt during LPS stimulation were significantly different from those in the control group; thus, P and ψ were corrected using D and W, respectively. Figure 8d shows the result before the correction and Figure 8e shows the result after the correction. The P-value of p-tyrosine indicated type 3 (passive) and could not be corrected.

Finally, we propose an emergent property score (Ep) as a method for evaluating emergent cellular responses, rather than classifying them into two-dimensional visual graphs. The Ep score is used as a guide for a cross-sectional comparison of observation events. Specifically, it is effective when a comparison of experimental systems in which stimulants are mixed is desired, such as when examining synergistic and/or additive effects. It is also useful for verifying the observation viewpoint, such as the oscillation signal. Further, it may be useful for assessing emergent cell responses when the antibodies used are the same in different experiments but the measuring instruments are different, although further study is needed to verify this. Ep is expressed as a continuous variable by integrating the absolute value of P with ψ. This has been corrected using both D and W. That is,

$$Ep = \psi * W * |P| * D.$$

Table 2 shows the Ep scores for the results obtained in the current study. Accordingly, Ep > 0 suggests that a parameter is robust (forms a hierarchy) and is involved in the characteristic events caused by the stimulant; and Ep < 0 suggests

Table 2. Emergent properties (Ep) score in various measurements.

cell	stimulants	control	parameter	Ep score[1]
HL60 (ec800)[2]				
	IFN-α, 100 U/mL, 30 min	0 min	p-STAT3	730
	G-CSF, 1 nM, 30 min	0 min	p-STAT3	-10,761
U937 (ec800)[2]				
	PMA, 100 ng/mL, 15 min	0 min	p-p65NF-κB	-1,549
	PMA, 100 ng/mL, 120 min	15 min	p-p65NF-κB	844
Monocytes in peripheral blood (FACSCanto II)[2]				
	LPS, 1 μg/mL, 30 min	Vehicle, 30 min	p-ERK1/2	-10,761
	LPS, 1 μg/mL, 30 min	Vehicle, 30 min	p-38MAPK	-11,214
	LPS, 1 μg/mL, 30 min	Vehicle, 30 min	p-Akt	8,095
Neutrophils in peripheral blood (FACSCanto II)[2]				
	IL-21, 1 nM, 30 min	Vehicle, 30 min	p-STAT3	-4398
	LPS, 1 μg/mL, 30 min	Vehicle, 30 min	p-STAT3	-891
	IL-21 + LPS, 30 min	Vehicle, 30 min	p-STAT3	-675
	IL-21, 1 nM, 30 min	Vehicle, 30 min	p-Akt	-13
	LPS, 1 μg/mL, 30 min	Vehicle, 30 min	p-Ak	1,128
	IL-21 + LPS, 30 min	Vehicle, 30 min	p-Ak	13,961
T cells in peripheral blood (FACSCanto II)[2]				
	IL-21, 1 nM, 30 min	Vehicle, 30 min	p-STAT3	50,153
	LPS, 1 μg/mL, 30 min	Vehicle, 30 min	p-STAT3	-71
	IL-21 + LPS, 30 min	Vehicle, 30 min	p-STAT3	51,600
	IL-21, 1 nM, 30 min	Vehicle, 30 min	p-Akt	-46
	LPS, 1 μg/mL, 30 min	Vehicle, 30 min	p-Ak	0
	IL-21 + LPS, 30 min	Vehicle, 30 min	p-Ak	-3

[1]When the event was not classified to Type 3 (Passive), Ep score were calculated using following formula:

Ep = ψ * W * | Pt | * D; D = $|\overline{MFI_t} - \overline{MFI_C}| \,/\, \overline{MFI_C}$; W = $|\overline{CV_t} - \overline{CV_C}| \,/\, \overline{CV_C}$

[2]The apparatus of flow cytometry for measurements are indicated in parentheses.

that the parameters are involved in the induction of other events or amplifying events caused by the stimulant. As an example, neutrophil stimulation with a mixture of IL-21 and LPS induced Ep > 0, while stimulation with IL-21 or LPS alone led to Ep < 0. It can hence be inferred that Akt and STAT3 may cooperate to induce characteristic events in neutrophils.

Discussion

In the current study, we proposed that cell response to signals might follow five patterns, determined by the measurement of MFI and CV values. A robust signaling pathway is recognized as a relative decrease in CV; hence, it is classed as "attractive" or "negative arbiter". A regulatory signal, which involves a relative increase in CV, is classed as "subsequent" and "countering". In addition, during the observation period of cell activation in the case of one-way signal activation (Figure 3), MFI and CV show a positive or negative correlation. Oscillating signaling pathways are composed of a "subsequent" pattern, and an intermediate pattern between "countering" and "negative arbiter" (Figure 4). A homeostatic signaling pathway is an oscillatory pathway between "passive" and "countering" patterns and is hence

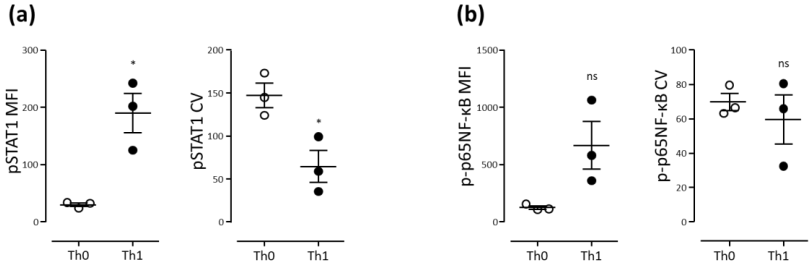

Figure S5. Analysis of STAT1 and NF-κB signaling pathways in Th0 and Th1 cells.
Splenocytes were stimulated with ovalbumin (OVA) for 7 days. After the stimulations (random and spontaneous T cell differentiation), the cells were fixed/permeabilized and stained with mAbs (V450-conjugated anti-mouse CD3 mAb, PE-Cy7-conjugated anti-mouse CD4 mAb, Alexa488-conjugated pSTAT1 mAb, Alexa647-conjugated p-p65 NF-κB mAb, and PE-conjugated anti-T-bet mAb or a mixture of PE-conjugated anti-T-bet mAb, anti-GATA3 mAb, anti-RORγt mAb, and anti-Bcl-6 mAb). The cells were analyzed by FCM (FACSCanto II). Th0 cell subset was gated as T-bet$^-$ GATA3$^-$ RORγt$^-$ Bcl-6$^-$ in CD3$^+$CD4$^+$ cells (open circle), and Th1 cell subset was gated as T-bet$^+$ in CD3$^+$CD4$^+$ cells (closed circle). MFI and CV of pSTAT1 (a) and p-p65 NF-κB (b) are presented. Data were obtained from three independent experiments, and the statistical significance were calculated by paired Student's *t*-test, $^*p < 0.05$.

[Procedures]

OT-II transgenic mice (OT-II mice), which express T cell receptor (TCR) α and β chains that recognize the MHC class II Ib-restricted ovalbumin (OVA) peptide (residues 323–339) in a C57BL/6J background, were kindly provided by Dr. W. Heath (WEHI, Melbourne, Australia). The mice were bred at the animal facilities of Yamagata University, Faculty of Medicine, under specific-pathogen-free conditions and were used for experiments at 6–12 weeks of age. The animal experiments were approved by the Animal Experiment Committee of Yamagata University, Faculty of Medicine (approval number, 31006). Spleens from OT-II mice were minced and homogenized, and the cell suspensions were suspended in RPMI1640 medium containing L-glutamine and 25 mM HEPES and supplemented with 10% (v/v) fetal calf serum (FCS), 50 μM 2-mercaptoethanol, 100 units/mL of penicillin, and 100 μg/mL of streptomycin. The cells (4×10^6 cells/mL) were incubated with OVA (0.2 mg/mL) for 7 days. After incubation, the cells (1 mL) were fixed with the addition of x5 Lyse/Fix buffer (0.2 mL) for 10 min at 37℃. The fixed cells were packed by centrifugation at 800 ×g for 1 min and then stocked in 90% methanol (0.3 mL/tube) at −20℃ until staining with antibodies: PE/Cy7-conjugated anti-mouse CD4 mAb (GK1.5), PE-conjugated anti-T-bet mAb (4B10), PE-conjugated anti-Bcl-6 mAb (7D1), and from BioLegend (San Diego, CA); V450-conjugated anti-mouse CD3 mAb (17A2), PE-conjugated anti-GATA3 mAb (L50-823), PE-conjugated anti-RORγt mAb (Q31-378), from BD Biosciences (Franklin Lakes, NJ). The cell samples were stained with mixture of anti-T-bet mAb, anti-Bcl-6 mAb, anti-GATA3 mAb, anti-RORγt mAb, anti-CD3 mAb and anti-CD4 mAb. The negative cells of T-bet, Bcl-6, GATA3, and RORγt in CD3$^+$CD4$^+$ cell population were considered as Th0 cells (undifferentiated T cells). For detection of Th1 cells, the cell samples were stained with anti-T-bet mAb, anti-CD3 mAb and anti-CD4 mAb. The T-bet positive cells in CD3$^+$CD4$^+$ cell population were gated as Th1 cells. During the cell staining, Alexa488-conjugated anti-pY701-STAT1 mAb (4a) and Alexa647-conjugated anti-pS536-NF-κBp65 rabbit mAb (93H1) were mixed with these antibodies.

observed as "passive", with a correlation between MFI and CV (Figure 5).

The theoretical hypothesis in this study needs to be verified. We are looking for a suitable verification method. As one of the verifications, we measured STAT1 and NF-κB in T cell differentiation. It is known that STAT1 is important a signal for inducing differentiation of T cells into Th1 (T-bet positive cells)[24]. Therefore, we compared the MFI and CV of pSTAT1 and p-p65NF-κB in cells differentiated into Th1 (supplemental Figure S5). As a result, pSTAT1 was Type 1 and p-p5NF-κB was Type 3. And the Ep of STAT1 was as high as 40,930. This result is one of the verifications for the theoretical hypothesis. I would like to repeat this kind of verification in the future.

In addition, if we can compare data in this study with some kind of "Gold Standard", the theoretical hypothesis will be validated. However, we have not been able to find a database of algorithms and ontology analysis that focuses on the fluctuation of phosphorylation signals. In the future, we would like

Supplementary Table S1. Type 3 (passive) can be separated from the other six types of cells transition using change in MFI or CV and correlation between MFI and CV.
NS, not significant.

Categories	Statistical change in MFI	Statistical change in CV	Correlation between MFI and CV	Speculative cells transition
Type 1/2	Increase	NS	NS	Intermediate between type 1 and 2 (mirror image of NF-κB in later phase)
Type 2/4	NS	Increase	NS	Perturbation by another basin (p-tyrosine)
Type 2/5	NS	NS	Positive correlation	Shuttling between type 2 and 5 (mirror image of homeostatic ERK1/2)
Type 3	NS	NS	NS	"Passive" as shown in Table 1
Type 1/4	NS	NS	Negative correlation	Shuttling between type 1 and 4 (Homeostatic ERK1/2)
Type 1/5	NS	Decrease	NS	Disappearance of perturbation by another basin (mirror image of p-tyrosine)
Type 4/5	Decrease	NS	NS	Intermediate between type 4 and 5 (NF-κB in later phase)

to examine a comprehensive analysis method that fits the theoretical hypothesis shown in this study.

Many researchers may wonder what a bimodal or distorted histogram may mean. In the current study, the shape of the histogram was topologically transformed into a simple shape, depending on the change in MFI and CV, as shown in Table 1. A bimodal or distorted histogram is considered to indicate an increase in CV. These histograms suggest that the cell population consists of several cell subsets, which differ with respect to the response to the stimulant.

The existence of a type 3 pattern with a negative correlation between MFI and CV (the homeostatic ERK pathway) allowed us to speculate that there is a mirror image of type 3 with a positive correlation between MFI and CV. Observation of an increase in CV with no change in MFI (the p-tyrosine experiment) also allowed us to speculate that there is a mirror image, i.e., a scenario with a decrease in CV without a change in MFI. Furthermore, observation of a decrease in MFI with no change in CV (p-p65NF-κB, late phase observations) prompted the speculation of the possibility of an increase in MFI without a change in CV. These patterns suggest that type 3 (passive) consists of six variations (Supplementary Table S1, Figure 6). It can be inferred that the six variations of type 3 are also elements of signal transduction pathways.

Whether this classification method can be applied to various measurement systems must be examined in the future. To discuss the advantages and problems of this method, the characteristics of the FCM measurement should be considered. For instance, FCM does not measure the absolute number of photons of fluorescence, and the detection sensitivity of the photomultiplier tube is adjusted so that all data fall within the measurement range before the measurement (in the case of a microscope, the magnification is adjusted for observation). To use simple imagery, let's image boxes arranged side by side, numbered in order. The numbers are the values on the horizontal axis of the histogram. The height of the histogram depends on the number of cells stored in the allocated box. When the number of photons released by one cell is relatively large, it is distributed to the box with a large number, and when the number of photons is small, it is distributed to the box with a small number. The number of boxes is limited and does not change during the measurement. Consequently, the difference in the number of photons released from one cell is measured as a relative value to the overall variation. The relative value is expressed as the MFI of the sample. When the detection sensitivity conditions of the photomultiplier tube are the same, stable MFI readings are obtained. If MFI is converted to an absolute quantity instead of a relative value,

it is necessary to use a standard product for each parameter. This is similar to other color-reaction measurement systems.

As another problem of FCM, the noise/signal (N/S) ratio differs depending on the fluorescent substance involved. In other words, the MFI value differs depending on the fluorescent substance. The N/S ratio of the fluorescent substance also affects determining the positive rate using the negative control staining. On the other hand, P obtained in the current study was not the positive rate using the threshold. Negative staining was not used as a control. The control value (MFI_c) was set as a condition similar to the tested condition (MFI_t), and the difference between MFI_t and MFI_c was calculated. As mentioned above, since MFI is a measured value whose relativity is already maintained at the time of measurement, the relative change in MFI can be stably estimated.

In the current study, P and ψ could be adjusted by using the correction values D and W, even if the labeled fluorescence and the measuring device were different. Furthermore, although the CV differs depending on the measuring device, the difference ψ ($CV_c - CV_t$) shows good reproducibility, as does the difference P ($MFI_t - MFI_c$). Since not many types of antibodies were examined herein, and the types of devices used were also limited, it remains unclear whether P and ψ can be applied in all scenarios. This study is not sufficient for mathematical generalization. Further experiments are needed to confirm the utility of the $P - \psi$ graph and Ep score. The graph and the score may be useful for comparing the attractivity of the observed parameters between different parameters.

It is difficult to study cell signaling in tissues using flow cytometry. This is because it takes several hours to process the enzymes that separates the cells from tissues. Artificial changes in the signal occur during the enzymatic treatment. The phosphorylation of signal transducers can not be used as a measurement parameter for applying the five types of cells transition in situ. Instead of the phosphorylation, cell membrane surface antigens or nuclear proteins may be suitable for a measurement parameter to apply the cells transition. Previously, we examined the variation of cell surface antigens and intracellular antigens using clinical blood samples after several hours from blood collections[25),26)]. We would like to carry out such verification in the future.

The cells transition, such as type 1 or type 5, is considered to be a robust signal response, so that the transition may be useful as an index for drug discovery. In addition, CV increases when the same cell population contains cell populations that respond differently. Previously, we reported that CV can be used to predict the prognosis of cancer[25)]. In addition, if immune cells are evaluated by the classification proposed in this study, they may be used for re-classification of syndromes or disease progression related to immune diseases.

To conclude, we here proposed a novel method for classifying signaling pathways using FCM. The contraction and fluctuation of cell clusters are useful for categorizing the signal characteristics. Previously, we reported that CV could be used for phosphorylated molecules and also for cell surface molecules[25),26)]. In addition, this method does not require a Bayesian approach or a diffusion map to supplement the missing values or cell fluctuations. Furthermore, it is possible to infer the elements of cell behavior without using ontological classification or module analysis based on known facts. This method is therefore highly effective for detecting event hierarchies based on the emergent properties of cells in various measurement systems.

Acknowledgments: We would like to thank Associate Professor Yutaro Obara (Department Pharmacology, Yamagata University Faculty of Medicine) for their valuable suggestions on ERK pathways. This research was funded by Grant-in-Aid for Scientific Research, grant number 22590432.

References

1. Krauss G.: Biochemistry of signal transduction and regulation. 2014
2. Yugi K, Kubota H, Hatano A, Kuroda S.: Trans-Omics: How To Reconstruct Biochemical Networks Across Multiple 'Omic' Layers. Trends Biotechnol 2016; 34: 276-290

3. Ohigashi I, Tanaka Y, Kondo K, Fujimori S, Kondo H, Palin AC, et al. : Trans-omics Impact of Thymoproteasome in Cortical Thymic Epithelial Cells. Cell Rep 2019; 29: 2901-2916 e2906
4. Perkel JM.: Single-cell analysis enters the multiomics age. Nature 2021; 595: 614-616
5. Becher B, Schlitzer A, Chen J, Mair F, Sumatoh HR, Teng KW, et al. : High-dimensional analysis of the murine myeloid cell system. Nat Immunol 2014; 15: 1181-1189
6. Becht E, McInnes L, Healy J, Dutertre CA, Kwok IWH, Ng LG, et al. : Dimensionality reduction for visualizing single-cell data using UMAP. Nat Biotechnol 2018
7. Kaneko K, Tsuda I.: Complex systems: chaos and beyond: a constructive approach with applications in life sciences. 2011
8. Kaneko K.: The challenges facing systemic approaches in biology: an interview with kunihiko kaneko. Front Physiol 2011; 2: 93
9. Kaneko K.: Life: An Introduction to Complex Systems Biology. 2006
10. Furusawa C, Kaneko K.: Formation of dominant mode by evolution in biological systems. Phys Rev E 2018; 97: 042410
11. Takeda Y, Nara H, Araki A, Asao H.: Human peripheral neutrophils express functional IL-21 receptors. Inflammation 2014; 37: 1521-1532
12. Takeda Y, Asao H, Wakabayashi I.: An Analysis of the Intracellular Signal Transduction of Peripheral Blood Leukocytes in Animal Models of Diabetes Using Flow Cytometry. Methods Mol Biol 2019; 1916: 177-193
13. Takeda Y, Nara H, Asao H.: Analysis of signal transducers using flow cytometry is useful for detection of contractive and fluctuating signals. Bulletin of the Yamagata University. Medical science : Yamagata medical journal 2017; 35: 21-32
14. Paszek P, Jackson DA, White MR.: Oscillatory control of signalling molecules. Curr Opin Genet Dev 2010; 20: 670-676
15. Juliana FM, Nara H, Onoda T, Rahman M, Araki A, Jin L, et al. : Apurinic/apyrimidinic endonuclease1/redox factor-1 (Ape1/Ref-1) is essential for IL-21-induced signal transduction through ERK1/2 pathway. Biochem Biophys Res Commun 2012; 420: 628-634
16. Zhao LJ, Wang W, Wang WB, Ren H, Qi ZT.: Involvement of ERK pathway in interferon alpha-mediated antiviral activity against hepatitis C virus. Cytokine 2015; 72: 17-24
17. Kamezaki K, Shimoda K, Numata A, Haro T, Kakumitsu H, Yoshie M, et al. : Roles of Stat3 and ERK in G-CSF signaling. Stem Cells 2005; 23: 252-263
18. Chambard JC, Lefloch R, Pouyssegur J, Lenormand P.: ERK implication in cell cycle regulation. Biochim Biophys Acta 2007; 1773: 1299-1310
19. Albeck JG, Mills GB, Brugge JS.: Frequency-modulated pulses of ERK activity transmit quantitative proliferation signals. Mol Cell 2013; 49: 249-261
20. Nick JA, Avdi NJ, Gerwins P, Johnson GL, Worthen GS.: Activation of a p38 mitogen-activated protein kinase in human neutrophils by lipopolysaccharide. J Immunol 1996; 156: 4867-4875
21. Guha M, Mackman N.: LPS induction of gene expression in human monocytes. Cell Signal 2001; 13: 85-94
22. Shankaran H, Wiley HS.: Oscillatory dynamics of the extracellular signal-regulated kinase pathway. Curr Opin Genet Dev 2010; 20: 650-655
23. Guha M, Mackman N.: The phosphatidylinositol 3-kinase-Akt pathway limits lipopolysaccharide activation of signaling pathways and expression of inflammatory mediators in human monocytic cells. J Biol Chem 2002; 277: 32124-32132
24. Takeda A, Hamano S, Yamanaka A, Hanada T, Ishibashi T, Mak TW, et al. : Cutting edge: role of IL-27/WSX-1 signaling for induction of T-bet through activation of STAT1 during initial Th1 commitment. J Immunol 2003; 170: 4886-4890
25. Kato T, Takeda Y, Ito H, Kurota Y, Yamagishi A, Sakurai T, et al. : GPI-80 as a Useful Index for Myeloid Cell Heterogeneity and a Potential Prognostic Biomarker for Metastatic Renal Cell Carcinoma. Tohoku J Exp Med 2019; 249: 203-212
26. Takeda Y, Kato T, Ito H, Kurota Y, Yamagishi A, Sakurai T, et al. : The pattern of GPI-80 expression is a useful marker for unusual myeloid maturation in peripheral blood. Clin Exp Immunol 2016; 186: 373-386